

3D Semantic Segmentation of Brain Tumor for Overall Survival Prediction

Rupal R. Agravat¹[0000-0003-1995-4149] and Mehul S. Raval¹[0000-0002-3895-1448]

Ahmedabad University, Ahmedabad, Gujarat, India
rupal.agravat@iet.ahduni.edu.in
mehul.raval@ahduni.edu.in

Abstract. Glioma, a malignant brain tumor, requires immediate treatment to improve the survival of patients. The heterogeneous nature of Glioma makes the segmentation difficult, especially for sub-regions like necrosis, enhancing tumor, non-enhancing tumor, and edema. Deep neural networks like full convolution neural networks and an ensemble of fully convolution neural networks are successful for Glioma segmentation. The paper demonstrates the use of a 3D fully convolution neural network with a three-layer encoder-decoder approach. The dense connections within the layer help in diversified feature learning. The network takes 3D patches from T_1 , T_2 , T_1c , and FLAIR modalities as input. The loss function combines dice loss and focal loss functions. The Dice similarity coefficient for training and validation set is 0.88, 0.83, 0.78 and 0.87, 0.75, 0.76 for the whole tumor, tumor core and enhancing tumor, respectively. The network achieves comparable performance with other state-of-the-art ensemble approaches. The random forest regressor trains on the shape, volumetric, and age features extracted from ground truth for overall survival prediction. The regressor achieves an accuracy of 56.8% and 51.7% on the training and validation sets.

Keywords: Brain Tumor Segmentation · Deep Learning · Dense Network · Overall Survival · Radiomics Features · Random Forest Regressor · U-net.

1 Introduction

Early-stage brain tumor diagnosis can lead to proper treatment planning, which improves patient survival chances. Out of all types of brain tumors, Glioma is one of the most life-threatening brain tumors. It occurs in the glial cells of the brain. Depending on its severity and aggressiveness, Glioma has grades ranging from I to IV. Grade I, II are Low-Grade Glioma (LGG), and grade III and IV are High-Grade Glioma (HGG). It can further be divided into constituent structures like - necrosis, enhancing tumor, non-enhancing tumor, and edema. The core consists of necrosis, enhancing tumor, non-enhancing tumor. In most cases LGG does not contain enhancing tumor, whereas HGG contains necrosis, enhancing,

and non-enhancing structures. Edema occurs from infiltrating tumor cells and biological response to the angiogenic and vascular permeability factors released by the spatially adjacent tumor cells[3]. Non-invasive Medical Resonance Imaging (MRI) is the most advisable imaging technique as it captures the functioning of soft tissue adequately compared to other imaging techniques. MR images are prone to inhomogeneity introduced by the surrounding magnetic field, which introduces the artifacts in the captured image. Besides, the appearance of various brain tissues is different in various modalities. Such issues increase the time in the study of the image.

The treatment planning is highly dependent on the accurate tumor structure segmentation, but due to heterogeneous nature of Glioma, the segmentation task becomes difficult. Furthermore, the human interpretation of the image is non-reproducible as well as dependent on expertise. It requires computer-aided MR image interpretation to locate the tumor. Also, even if the initially detected tumor is completely resected, such patients have poor survival prognosis, as metastases may still redevelop. It leads to an open question about overall survival prediction.

Authors in [1] discussed the basic, generative, and discriminative techniques for brain tumor segmentation. Nowadays, Deep Neural Network (DNN) has gained more attention for the segmentation of biological images. The Convolution Neural Networks (CNN), like DeepMedic [15], U-net [22], V-Net [20], SegNet [5], ResNet [12], DenseNet [13] give state-of-the-art results for semantic segmentation. Out of all these methods, U-net is a widely accepted end-to-end segmentation architecture for brain tumors. U-net is an encoder-decoder architecture, which reduces the size of feature maps to half and doubles the number of feature maps at every encoder layer. The process is reversed at every decoder layer. The skip connections between the peer layers of U-net help in proper feature reconstruction.

1.1 Literature Review: BraTS 2019

Segmentation Authors in [14] used the ensemble of twelve encoder-decoder models, where each model is made up of a cascaded network. The first network in a model finds the coarse segmentation, which was given as input in the second network, and the input images to predict all the labels. The network losses combine at different stages for better network parameter tuning. The Dice Similarity Coefficient (DSC) for the validation set is 0.91, 0.87, 0.80 for Whole Tumor (WT), Tumor Core (TC), and Enhancing Tumor (ET), respectively.

In [28], authors applied various data processing methods, network design methods, and optimization methods to learn the segmentation labels at every iteration. The student models combined at the teacher-level model with successive output merging. The loss function is the combination of dice loss and cross-entropy loss for the networks trained on various input patch sizes. The method achieved the DSC of 0.91, 0.84, and 0.75 for WT, TC, and ET, respectively.

The approach demonstrated in [18] used thirty Heteroscedastic classification models to find the variance of all the models for the ensemble. The focal loss forms the loss function. Various post-processing techniques were applied to fine-tune the network segmentation. The DSC achieved for the approach was 0.91, 0.83, and 0.77 for WT, TC, and ET.

Authors in [23] used fifteen 2D FCNN models working in parallel on axial, coronal and sagittal views of images. The approach used in [11] focused on the attention mechanism applied for the ensemble of four 3D FCNN models. In [16], authors used the ensemble of four 2D FCNN models working on different sets of images based on the size of the tumor.

Survival Prediction Authors in [2] implemented 2D U-net with dense modules at the encoder part and convolution modules at the decoder part along with focal loss function at training time. The segmentation results fed into Random Forest Regressor(RFR) to predict the Overall Survival (OS) of the patients. The RFR trains on the age, shape, and volumetric features extracted from the ground truth provided with the training dataset. They achieved 58.6% OS accuracy on the validation set.

Authors in [27] used vanilla U-net and U-net with attention blocks to make the ensemble of six models based on various input patches and the presence/absence of attention blocks. The linear regressor trains selected radiomics features along with the relative invasiveness coefficient. The DSC achieved on the validation set was 0.90, 0.83, and 0.79 for WT, TC, and ET, respectively, and the OS accuracy was 59%.

Authors in [10] implemented the ensemble of six models, which are the variation of U-net with different patch sizes, feature maps with several layers in the encoder-decoder architecture. For OS prediction, six features were extracted from the segmentation results to train the linear regression. The DSC achieved on the validation set was 0.91, 0.80, and 0.74 for WT, TC, and ET, and the OS accuracy was 31%.

Authors in [26] used the U-net variation, where the additional branch of prediction uses Variational Encoder. The OS prediction used the volumetric and age features to train ANN with two layers, each with 64 neurons.

Except the approach demonstrated in [2,26], all the other approaches use an ensemble of the segmentation prediction networks. There are certain disadvantages of ensemble approaches: (1) ensemble methods are usually computationally expensive. Therefore, they add learning time, and memory constraints to the problem, (2) using ensemble methods reduces the model interpretability due to increased complexity and makes it very difficult to understand.

The focus of this paper is to develop a robust 3D fully convolutional neural network (FCNN) for tumor segmentation along with RFR [2] to predict OS of high grade glioma (HGG) patients. The remaining paper is as follows: section 2 focuses on the BraTS 2020 dataset, section 3 demonstrates the proposed methods for tumor segmentation and OS prediction, section 4 provides implementation

details, and section 5 discusses the results followed by the conclusion and future work.

2 Dataset

The dataset [8,9,19] contains 293 HGG and 76 LGG pre-operative scans in four Magnetic Resonance Images (MRI) modalities, which are T_1 , T_2 , T_1c and FLAIR. One to four raters have segmented the images using the same annotation tool to prepare the ground truths. The annotations were approved by experienced neuro-radiologists [6,7]. Annotations have the enhancing tumor (ET label 4), the peritumoral edema (ED label 2), and the necrotic and non-enhancing tumor core (NCR/NET label 1). The T_2 , T_1c and FLAIR images of a single scan are co-registered with the anatomical template of T_1 image of the same scan. All the images are interpolated to the same resolution (1mm x 1mm x 1mm), and skull-stripped. Features like age, survival days and resection status for 237 HGG scans are provided separately for OS. The validation and test datasets consist of 125 and 166 MRI scans respectively, with the same pre-processing. The dataset includes age and resection status for all the sets along with survival days for the training set.

3 Proposed Method

3.1 Task 1: Tumor Segmentation

A FCNN provides end-to-end semantic segmentation for the input of the arbitrary size and learns global information related to it. Moreover, the 3D FCNN gathers spatial relationships between the voxels. Our network is an extension of our previous work proposed in [2], where the network had poorly performed on validation set and test set. The network overfitted the training set and could not learn the 3D voxel relationship. The proposed work includes 3D modules with increased network depth. The network uses three-layer encoder-decoder architecture with dense connections between the convolution layers and skip-connections across peer layers. The network is as shown in Fig. 1. The Batch Normalization (BN) and Parametric ReLU (PReLU) activation function follow the convolution layer in each dense module.

Dense connections between the layers in the dense module allows to obtain additional inputs(collective knowledge) from all earlier layers and passes on its feature-maps to all subsequent layers. It allows the gradient to flow to the earlier layers directly, which provides in-depth supervision on preceding layers by the classification layer. Also, dense connections provide diversified features to the layers, which leads to detailed pattern identification capabilities. The layers generate 64, 128 and 256 feature maps and the bottleneck layer generates 512 feature maps. The 1x1x1 convolution at the end generates a single probability map for multi-class classifications.

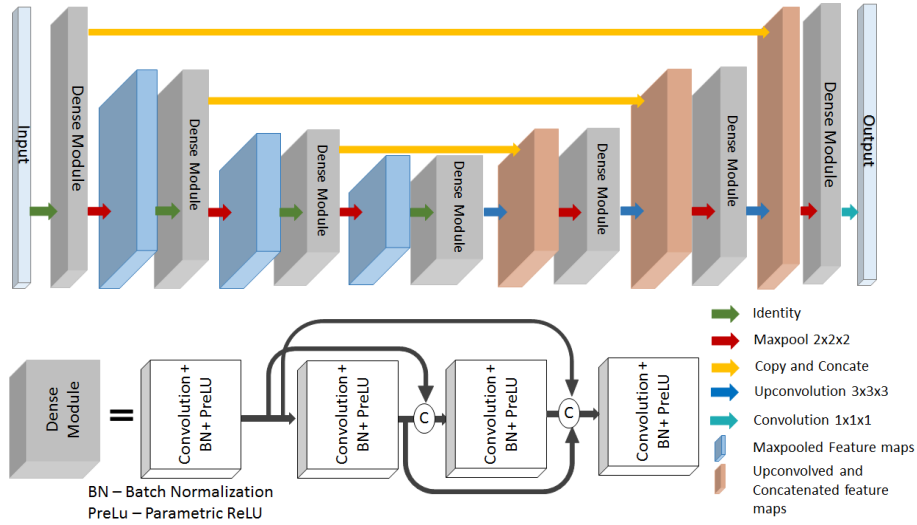


Fig. 1: The proposed 3D encoder-decoder FCNN.

Brain tumor segmentation task deals with a highly imbalanced dataset where tumorous slices are less than non-tumorous slices; such an imbalance dataset reduces network accuracy. Two approaches deal with the issue: 1) The patch-based input to the network guarantees that the network does not overlearn the background voxels, 2) the network trains with the combination of the following loss functions.

- Soft Dice Loss: is a measure to find overlap between two regions.

$$\text{Soft Dice Loss} = 1 - \frac{2 \sum_{\text{voxels}} y_{\text{true}} y_{\text{pred}}}{\sum_{\text{voxels}} y_{\text{pred}}^2 + \sum_{\text{voxels}} y_{\text{true}}^2}$$

y_{true} represents ground truth and y_{pred} represents network output probability. The dice loss function directly considers the predicted probabilities without converting them into binary output. The numerator provides standard correct predictions between input and target, whereas the denominator provides individual separate correct predictions. This ratio normalizes the loss according to the target mask and allows learning even from the minimal spatial representation of the target mask.

- Focal Loss[17]: It is dependent on the network probability p_t . It balances negative and positive samples by tuning weighting parameter α . It also deals with easy and hard examples by tuning the focusing parameter γ .

$$FL(p_t) = -\alpha_t (1 - p_t)^\gamma \log(p_t) \quad (1)$$

The modulating factor $(1 - p_t)^\gamma$ adjusts the rate at which easy examples are down-weighted.

3.2 Task 2: Overall Survival Prediction

OS prediction deals with predicting the number of days for which patients survive after the tumor is resected and proper post-operative treatment given. We have used the following features to train RFR:

- **Statistical Features:** the amount of edema, amount of necrosis, amount of enhancing tumor, the extent of tumor and proportion of tumor.
- **Radiomic Features[25] for necrosis:** Elongation, flatness, minor axis length, primary axis length, 2D diameter row, 2D diameter column, sphericity, surface area, 2D diameter slice, 3D diameter.
- **Age**(available with BraTS dataset).

Necrosis plays a significant role in the treatment of tumors. Gross Total Resection(GTR) of necrosis is comparatively easy vis a vis enhancing tumor. Considering this, shape features of necrosis are extracted using a radiomics package [25]. In addition to these features, whole tumor statistical features from the segmentation results and age are considered to train RFR.

4 Implementation Details

4.1 Pre-processing

Pre-processing boosts network training and improves performance. All four modality images are biased field corrected followed by denoising, and Z-score normalization on individual MR sequence is applied where each sequence was subtracted by its mean from the data and divided by its standard deviation. Data augmentation happens by flipping the patches around the vertical axis.

4.2 Training

Input to the network is patches of size 64x64x64 from four modalities (T1, T2, T1c, FLAIR). The network trains on the entire training image dataset. The network uses the combination of two loss functions: 1) dice loss function and 2) focal loss function with $\alpha = 1$ and $\gamma = 2$. The network trains for 610 epochs with batch size 1. The batch normalization with batch size 1 does not speed up the network learning but helps during testing, where it uses the statistics of the batch rather than the running statistics. This layer normalization approach [4] normalizes each feature map with its own mean and standard deviation.

The sliding window approach provides the output for each subject. The stride size is reduced to half of the training window size to overcome the boundary voxels' unstable prediction issue. The output of the original patch and flipped patch is predicted and averaged to generate the final output. The prediction of a single image takes around one minute.

4.3 Post-processing

The post-processing includes two methods: 1) The connected component analysis (CCA) removes the tumor with a volume less than thousand voxels, 2) enhancing tumor is formed in the surrounding of the necrosis, and its size cannot be very small in HGG. Such small size enhancing tumor is converted to necrosis. The empirically chosen threshold for the conversion is three hundred.

5 Results

5.1 Segmentation

The achieved DSC, sensitivity, specificity and Hausdorff95 for training set is in Table 1, and for the validation set in Table 2. The results shows the improvement with post-processing, hence the test set results are generated with post-processing as shown in Table 3.

Table 1: Various evaluation measures for BraTS 2020 training set.

Evaluation Measure	Statistics	Without post-process			With post-process		
		ET	WT	TC	ET	WT	TC
DSC	Mean	0.757	0.881	0.831	0.782	0.882	0.832
	StdDev	0.267	0.115	0.191	0.246	0.116	0.191
	Median	0.863	0.919	0.908	0.872	0.919	0.910
	25quantile	0.751	0.860	0.802	0.779	0.862	0.805
	75quantile	0.906	0.941	0.943	0.912	0.943	0.944
Sensitivity	Mean	0.759	0.846	0.802	0.782	0.844	0.801
	StdDev	0.272	0.156	0.209	0.252	0.158	0.209
	Median	0.858	0.896	0.883	0.864	0.896	0.883
	25quantile	0.748	0.797	0.763	0.762	0.795	0.763
	75quantile	0.921	0.946	0.931	0.925	0.945	0.931
Specificity	Mean	0.999	0.999	0.999	0.999	0.999	0.999
	StdDev	0.000	0.000	0.000	0.000	0.000	0.000
	Median	0.999	0.999	0.999	0.999	0.999	0.999
	25quantile	0.999	0.999	0.999	0.999	0.999	0.999
	75quantile	0.999	0.999	0.999	0.999	0.999	0.999
Hausdorff95	Mean	31.531	06.508	07.275	29.274	06.232	06.999
	StdDev	95.090	08.588	10.946	94.956	08.134	20.507
	Median	01.732	03.606	03.606	01.414	03.464	03.317
	25quantile	01.414	02.236	02.000	01.000	02.236	02.000
	75quantile	04.123	07.071	08.602	03.162	06.939	07.874

The proposed model outperforms some of the ensemble approaches which is shown in Table 4. Fig. 2 shows the successful segmentation of the tumor.

Table 2: Various evaluation measures for BraTS 2020 validation set.

Evaluation Measure	Statistics	Without post-process			With post-process		
		ET	WT	TC	ET	WT	TC
DSC	Mean	0.686	0.876	0.725	0.763	0.873	0.753
	StdDev	0.307	0.093	0.284	0.259	0.098	0.263
	Median	0.835	0.914	0.866	0.852	0.908	0.878
	25quantile	0.617	0.863	0.595	0.751	0.856	0.711
	75quantile	0.889	0.932	0.924	0.899	0.935	0.926
Sensitivity	Mean	0.704	0.858	0.674	0.759	0.847	0.713
	StdDev	0.322	0.138	0.312	0.273	0.149	0.288
	Median	0.853	0.901	0.819	0.852	0.897	0.841
	25quantile	0.595	0.826	0.432	0.715	0.809	0.606
	75quantile	0.926	0.952	0.915	0.933	0.954	0.921
Specificity	Mean	0.999	0.999	0.999	0.999	0.999	0.999
	StdDev	0.000	0.000	0.000	0.001	0.000	0.000
	Median	0.999	0.999	0.999	0.999	0.999	0.999
	25quantile	0.999	0.999	0.999	0.998	0.999	0.999
	75quantile	0.999	0.999	0.999	0.999	0.999	0.999
Hausdorff95	Mean	43.635	09.475	14.538	27.704	07.038	10.873
	StdDev	109.143	15.215	38.067	90.918	09.348	33.823
	Median	02.828	04.000	05.099	02.236	03.742	04.690
	25quantile	01.414	02.236	02.236	01.414	02.449	02.236
	75quantile	10.770	07.550	10.724	04.242	06.480	11.045

The false positive segmentation voxels are removed in the post-processing. The network fails to segment the tumor for some HGG images and many LGG images. One such segmentation failure is shown in Fig. 3. The failure of the network is observed for: 1) small size of the entire tumor, 2) small size of necrosis, and 3) absence/small size of enhancing tumor. Fig. 4 depicts the box plot of the evaluation metrics, where the red marked cases shows the segmentation failure.

5.2 OS Prediction

The RFR trains on features extracted from the 213 ground truth images. In the trained RFR, features of network segmented images predict OS days. If the network fails to identify / segment necrosis from the image, then the feature extractor considers the absence of the necrosis and marks all the features except age as zero. OS accuracy on training, validation and test datasets for the images with GTR resection status is in Table 5.

The reduced performance of RFR on validation and test sets shows that it overfits the training dataset. Still, its performance is comparable with other approaches as shown in Table 6.

Table 3: Various evaluation measures for BraTS 2020 test set.

Evaluation Measure	Statistics	With Post-process		
		ET	WT	TC
DSC	Mean	0.779	0.875	0.815
	StdDev	0.232	0.112	0.250
	Median	0.847	0.910	0.913
	25quantile	0.760	0.855	0.833
	75quantile	0.908	0.935	0.948
Sensitivity	Mean	0.809	0.863	0.817
	StdDev	0.245	0.136	0.244
	Median	0.896	0.910	0.908
	25quantile	0.785	0.823	0.795
	75quantile	0.940	0.947	0.952
Specificity	Mean	0.999	0.999	0.999
	StdDev	0.000	0.001	0.001
	Median	0.999	0.999	0.999
	25quantile	0.999	0.999	0.999
	75quantile	0.999	0.999	0.999
Hausdorff95	Mean	27.078	08.302	21.611
	StdDev	92.554	30.007	74.651
	Median	01.732	03.464	03.162
	25quantile	01.103	02.000	01.799
	75quantile	02.734	06.164	07.858

According to the study [24], gender plays a vital role in response to tumor treatment. The females respond to the post-operative treatment better compared to males, which improves their life expectancy. The inclusion of the ‘gender’ feature into the existing feature list can significantly improve OS accuracy.

6 Conclusion

The proposal uses three-layer deep 3D U-net based encoder-decoder architecture for semantic segmentation. Each encoding and decoding layer module incorporates dense connections which allow the diversified feature learning and gradient propagation to the initial layers. The patch selection and loss function approaches improved the performance of the network. The pre-processing, post-processing and patch selection methods play vital role in the robust performance of the network. The network outperforms some of the state-of-the-art ensemble approaches. The network fails where the size of either the entire tumor or its sub-component (necrosis and enhancing tumor) is comparatively small. The smaller subcomponent size is observed in LGG cases where the network fails significantly. The age, statistical, and necrosis shape features of the ground truth train RFR with five-fold cross-validation for OS prediction. Later, network segmentation for

Table 4: DSC comparison with state-of-art ensemble approaches.

Ref.	Type of Network	No. of Networks	DSC		
			ET	WT	TC
[11]	3D FCNN	4	0.67	0.87	0.73
[16]	2D FCNN	4	0.68	0.84	0.73
[23]	2D FCNN	15	0.71	0.85	0.71
Proposed	3D FCNN	1	0.76	0.87	0.75

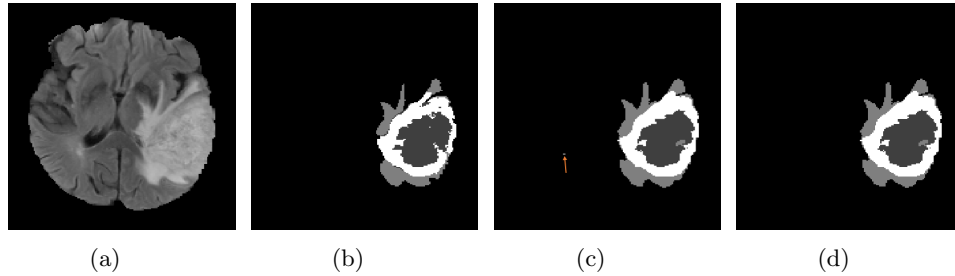


Fig. 2: Correct segmentation results of the network (a) FLAIR slice (b) Ground truth (c) Segmentation without post-processing (d) Segmentation after post-processing.

cases with GTR tests RFR for OS prediction. The RFR performs better than other state-of-the-art approaches which use linear regression and ANN.

Acknowledgement

The authors would like to thank NVIDIA Corporation for donating the Quadro K5200 and Quadro P5000 GPU used for this research, Dr. Krutarth Agravat (Medical Officer, Essar Ltd) for clearing our doubts related to medical concepts, Ujjawal Baid for his fruitful discussion in network selection. The authors acknowledge continuous support from Professor Sanjay Chaudhary, Professor N. Padmanabhan, and Professor Manjunath Joshi.

Table 5: OS accuracy for BraTS 2020 training, validation and test datasets.

Dataset	Accuracy	MSE	MedianSE	StdSE	SpearmanR
Training	0.568	083165.963	21481.525	0181697.874	0.596
Validation	0.517	116083.477	43974.090	0168176.159	0.217
Test	0.477	382492.357	46612.810	1081670.063	0.333

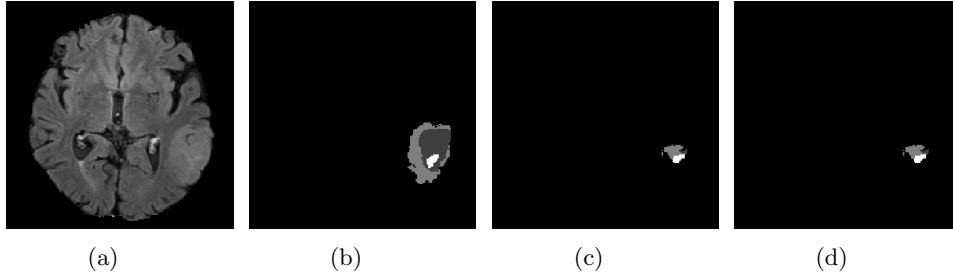


Fig. 3: Incorrect segmentation results of the network (a) FLAIR slice (b) Ground truth (c) Segmentation without post-processing (d) Segmentation after post-processing.

Table 6: Comparative analysis of OS accuracy on BraTS 2019 validation set.

Ref.	Approach	# features	Accuracy (%)
[10]	Linear Regression	9	31.0
[21]	Linear Regression	NA	51.5
[26]	Artificial Neural Network	7	45.0
Proposed	RFR	18	51.7

References

1. Agravat, R.R., Raval, M.S.: Deep learning for automated brain tumor segmentation in mri images. In: *Soft Computing Based Medical Image Analysis*, pp. 183–201. Elsevier (2018)
2. Agravat, R.R., Raval, M.S.: Brain tumor segmentation and survival prediction. In: *International MICCAI Brainlesion Workshop*. pp. 338–348. Springer (2019)
3. Akbari, H., Macyszyn, L., Da, X., Wolf, R.L., Bilello, M., Verma, R., O’Rourke, D.M., Davatzikos, C.: Pattern analysis of dynamic susceptibility contrast-enhanced mr imaging demonstrates peritumoral tissue heterogeneity. *Radiology* **273**(2), 502–510 (2014)
4. Ba, J.L., Kiros, J.R., Hinton, G.E.: Layer normalization. arXiv preprint arXiv:1607.06450 (2016)
5. Badrinarayanan, V., Kendall, A., Cipolla, R.: Segnet: A deep convolutional encoder-decoder architecture for image segmentation. *IEEE transactions on pattern analysis and machine intelligence* **39**(12), 2481–2495 (2017)
6. Bakas, S., Akbari, H., Sotiras, A., Bilello, M., Rozycki, M., Kirby, J., Freymann, J., Farahani, K., Davatzikos, C.: Segmentation labels and radiomic features for the pre-operative scans of the tcga-gbm collection. *the cancer imaging archive* (2017)
7. Bakas, S., Akbari, H., Sotiras, A., Bilello, M., Rozycki, M., Kirby, J., Freymann, J., Farahani, K., Davatzikos, C.: Segmentation labels and radiomic features for the pre-operative scans of the tcga-lgg collection. *The Cancer Imaging Archive* **286** (2017)

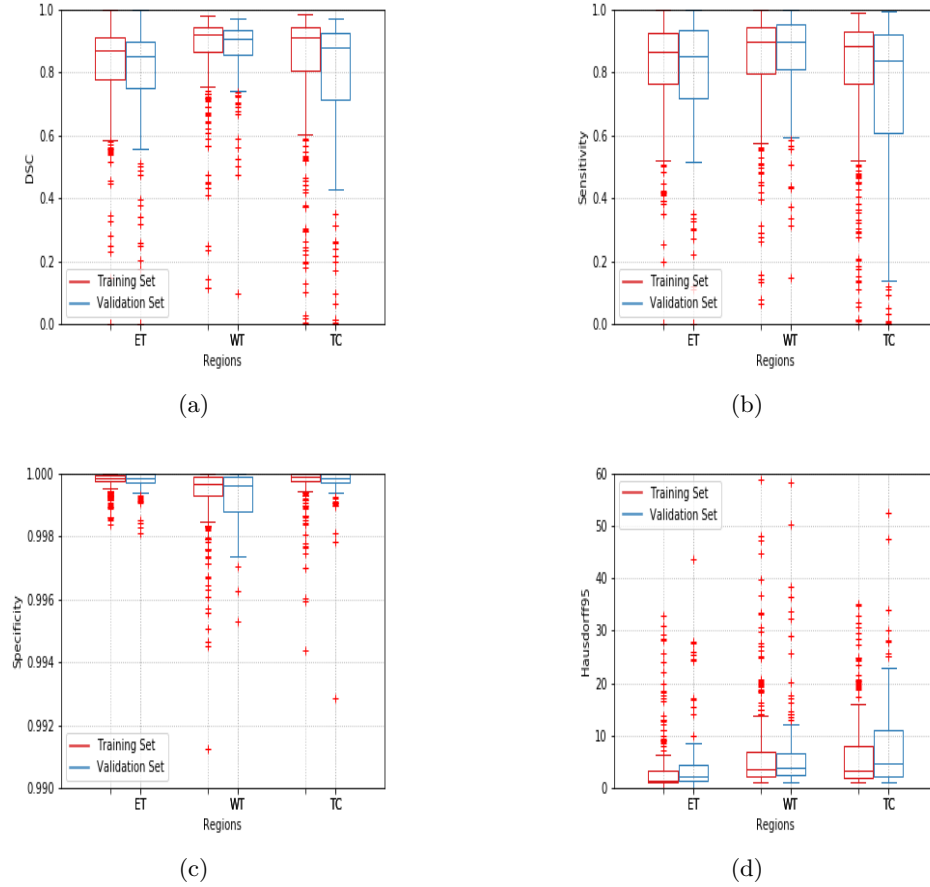


Fig. 4: The box plot (a) DSC (b) Sensitivity (c) Specificity (d) Hausdorff95

8. Bakas, S., Akbari, H., Sotiras, A., Bilello, M., Rozycki, M., Kirby, J.S., Freymann, J.B., Farahani, K., Davatzikos, C.: Advancing the cancer genome atlas glioma mri collections with expert segmentation labels and radiomic features. *Scientific data* **4**, 170117 (2017)
9. Bakas, S., Reyes, M., Jakab, A., Bauer, S., Rempfler, M., Crimi, A., Shinohara, R.T., Berger, C., Ha, S.M., Rozycki, M., et al.: Identifying the best machine learning algorithms for brain tumor segmentation, progression assessment, and overall survival prediction in the brats challenge. *arXiv preprint arXiv:1811.02629* (2018)
10. Feng, X., Dou, Q., Tustison, N., Meyer, C.: Brain tumor segmentation with uncertainty estimation and overall survival prediction. In: *International MICCAI Brainlesion Workshop*. pp. 304–314. Springer (2019)
11. Guo, X., Yang, C., Ma, T., Zhou, P., Lu, S., Ji, N., Li, D., Wang, T., Lv, H.: Brain tumor segmentation based on attention mechanism and multi-model fusion. In: *International MICCAI Brainlesion Workshop*. pp. 50–60. Springer (2019)

12. He, K., Zhang, X., Ren, S., Sun, J.: Deep residual learning for image recognition. In: Proceedings of the IEEE conference on computer vision and pattern recognition. pp. 770–778 (2016)
13. Iandola, F., Moskewicz, M., Karayev, S., Girshick, R., Darrell, T., Keutzer, K.: Densenet: Implementing efficient convnet descriptor pyramids. arXiv preprint arXiv:1404.1869 (2014)
14. Jiang, Z., Ding, C., Liu, M., Tao, D.: Two-stage cascaded u-net: 1st place solution to brats challenge 2019 segmentation task. In: Brainlesion: Glioma, Multiple Sclerosis, Stroke and Traumatic Brain Injuries: 5th International Workshop, BrainLes 2019, Held in Conjunction with MICCAI 2019, Shenzhen, China, October 17, 2019, Revised Selected Papers, Part I 5. pp. 231–241. Springer International Publishing (2020)
15. Kamnitsas, K., Ledig, C., Newcombe, V.F., Simpson, J.P., Kane, A.D., Menon, D.K., Rueckert, D., Glocker, B.: Efficient multi-scale 3d cnn with fully connected crf for accurate brain lesion segmentation. *Medical image analysis* **36**, 61–78 (2017)
16. Kotowski, K., Nalepa, J., Dudzik, W.: Detection and segmentation of brain tumors from mri using u-nets. In: International MICCAI Brainlesion Workshop. pp. 179–190. Springer (2019)
17. Lin, T.Y., Goyal, P., Girshick, R., He, K., Dollár, P.: Focal loss for dense object detection. In: Proceedings of the IEEE international conference on computer vision. pp. 2980–2988 (2017)
18. McKinley, R., Rebsamen, M., Meier, R., Wiest, R.: Triplanar ensemble of 3d-to-2d cnns with label-uncertainty for brain tumor segmentation. In: International MICCAI Brainlesion Workshop. pp. 379–387. Springer (2019)
19. Menze, B.H., Jakab, A., Bauer, S., Kalpathy-Cramer, J., Farahani, K., Kirby, J., Burren, Y., Porz, N., Slotboom, J., Wiest, R., et al.: The multimodal brain tumor image segmentation benchmark (brats). *IEEE transactions on medical imaging* **34**(10), 1993–2024 (2014)
20. Milletari, F., Navab, N., Ahmadi, S.A.: V-net: Fully convolutional neural networks for volumetric medical image segmentation. In: 2016 Fourth International Conference on 3D Vision (3DV). pp. 565–571. IEEE (2016)
21. Pei, L., Vidyaratne, L., Rahman, M.M., Shboul, Z.A., Iftekharruddin, K.M.: Multimodal brain tumor segmentation and survival prediction using hybrid machine learning. In: International MICCAI Brainlesion Workshop. pp. 73–81. Springer (2019)
22. Ronneberger, O., Fischer, P., Brox, T.: U-net: Convolutional networks for biomedical image segmentation. In: International Conference on Medical image computing and computer-assisted intervention. pp. 234–241. Springer (2015)
23. Starke, S., Eckert, C., Zwanenburg, A., Speidel, S., Löck, S., Leger, S.: An integrative analysis of image segmentation and survival of brain tumour patients. In: International MICCAI Brainlesion Workshop. pp. 368–378. Springer (2019)
24. Sun, T., Plutynski, A., Ward, S., Rubin, J.B.: An integrative view on sex differences in brain tumors. *Cellular and molecular life sciences* **72**(17), 3323–3342 (2015)
25. Van Griethuysen, J.J., Fedorov, A., Parmar, C., Hosny, A., Aucoin, N., Narayan, V., Beets-Tan, R.G., Fillion-Robin, J.C., Pieper, S., Aerts, H.J.: Computational radiomics system to decode the radiographic phenotype. *Cancer research* **77**(21), e104–e107 (2017)
26. Wang, F., Jiang, R., Zheng, L., Meng, C., Biswal, B.: 3d u-net based brain tumor segmentation and survival days prediction. In: International MICCAI Brainlesion Workshop. pp. 131–141. Springer (2019)

27. Wang, S., Dai, C., Mo, Y., Angelini, E., Guo, Y., Bai, W.: Automatic brain tumour segmentation and biophysics-guided survival prediction. arXiv preprint arXiv:1911.08483 (2019)
28. Zhao, Y.X., Zhang, Y.M., Liu, C.L.: Bag of tricks for 3d mri brain tumor segmentation. In: International MICCAI Brainlesion Workshop. pp. 210–220. Springer (2019)